SEMI-AUTOMATIC LYMPH NODE SEGMENTATION IN LN-MRI

G. Unal[a], G. Slabaugh[a], A. Ess[b], A. Yezzi[c], T. Fang[a], J. Tyan[a], M. Requardt[d], R. Krieg[d], R. Seethamraju[e], M. Harisinghani[f], R. Weissleder[f]

[a] Siemens Corporate Research
Intelligent Vision and Reasoning
Princeton NJ, USA

[b] Swiss Federal Institute ETH
Computer Science Department
Zurich, Switzerland

[e] Siemens Medical Solutions
Med-MR
Malvern PA, USA

[c] Georgia Institute of Technology
School of ECE
Atlanta GA, USA

[d] Siemens Med-MR
Medical Solutions
Erlangen, Germany

[f] Center For Molecular Imaging Research
Massachusetts General Hospital, Harvard University
Boston MA, USA

ABSTRACT

Accurate staging of nodal cancer still relies on surgical exploration because many primary malignancies spread via lymphatic dissemination. The purpose of this study was to utilize nanoparticle-enhanced lymphotropic magnetic resonance imaging (LN-MRI) to explore semi-automated noninvasive nodal cancer staging. We present a joint image segmentation and registration approach, which makes use of the problem specific information to increase the robustness of the algorithm to noise and weak contrast often observed in medical imaging applications. The effectiveness of the approach is demonstrated with a given lymph node segmentation problem in post-contrast pelvic MRI sequences.

Index Terms— biomedical image processing, image segmentation, biomedical magnetic resonance imaging, medical diagnosis

1. INTRODUCTION

Accurate staging of nodal cancer still relies on surgical exploration because many primary malignancies spread via lymphatic dissemination [1]. Particularly, accurate detection of lymph-node metastases in prostate cancer is an essential component of the approach to treatment [2]. MR nodal staging with lymphotropic magnetic nanoparticles (LN-MRI) has the potential to provide highly accurate non-invasive cancer staging. Images are currently assessed by qualitative visual analysis or by quantitative measurements with manual outlining. These approaches are laborious and impractical given the large number of lymph nodes. A practical solution to the problem is an automated process that can quickly and accurately support the physician in gathering the disease specific information from the magnetic resonance images.

The problem addressed in this paper is: given high resolution MR images with nanoparticles, to segment lymph nodes using computer algorithms and extract lymph node features for classification. The challenge of the problem is that the appearance, geometry, and location of lymph nodes have a huge variation over the MR images. Fig. 1 shows properties of benign and malignant nodes after administration of LN. The segmentation algorithm has to account for these variations in delineation of lymph nodes. The feature extraction algorithm should then identify discriminative features for a subsequent node classification. Complete solutions for an automated process currently do not exist.

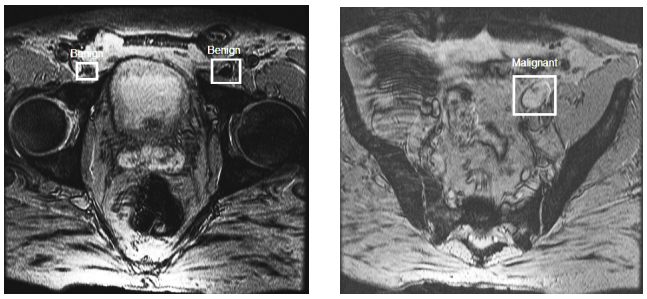

Fig. 1. MR images obtained after the contrast agent administration of results in a homogeneous and low signal intensity for benign lymph nodes (left),and a high intensity for a malignant lymph node (right).

An automatic or semi–automatic detection of anatomic structures provides faster and more precise diagnostic information to clinicians than manual outlining, and therefore increases the efficiency of the clinical work–flow. In the given lymph node detection in LN-MRI, multiple MR image sequences such as pre- and post-contrast agent images, different settings such as T2-, T2*-, and T1-weighted are available. In such situations, a detection usually refers to a segmentation for outlining a target structure and a registration in the presence of multiple images. Deformable models have been popular in medical image segmentation problems, see [3] for a survey. Medical images present a challenge to most segmentation algorithms due to clutter from the surrounding structures and noise inherent to medical imaging equipment, therefore shape priors are usually incorporated. Specifically, an ellipse is a powerful parametric form used in many computer vision tasks [4, 5]. A parametric maximum likelihood

fit to the medical data, particularly cardiac scintigrams, using an ellipse parameterization was developed in [6]. Other parametric approaches to segmentation include Fourier descriptors in [7], and spherical harmonics in [8]. For registration of medical structures, a tremendous amount of work has been done, see [9]. Recently, there has been an interest in combining segmentation and registration problems due to their strong interdependence [10, 11, 12, 13, 14, 15].

Our contribution in this study is a problem specific semi-automatic lymph node segmentation and feature extraction system, which couples the information from MR T2- and multiple T2*-weighted images for a joint segmentation and registration. In this way, our method utilizes all the information available in multiple images segmenting the target structure and registering it simultaneously in all images, thereby accounting for missing and weak information in some modalities. We hence simultaneously capture the boundaries of the lymph node in all the volumes. For surgical planning, we obtain a segmentation in three-dimensions and output the final lymph node surface for visualization along with the vascular anatomy using the T1 volume. Later, we automatically extract lymph node features that are explained in the work of Harisinghani&Weissleder [1], for lymph node classification.

In Fig. 2, a lymph node appears as a roughly homogeneous region on a T2–weighted MR image sequence, whereas the same node shows hardly visible boundary characteristics with no difference in the region information of its inside from outside on the T2*-MR images. An uncoupled segmentation is likely to fail due to an expected mis-registration among the different sequences although they were acquired during the same scan study, and due to missing information (Fig. 2a). The coupling of the information from multi-modal images through a joint segmentation and registration is therefore important (Fig. 2b). Utilization of prior information on such a challenging problem is critical, however, we did not resort to training since a common general shape of lymph nodes is hardly existent. On the other hand, an ellipse being a powerful approximator for shapes led us to make use of this parametric form for our multiple registration and segmentation problem.

The organization of the paper is as follows: we present the ellipse evolution models for joint registration and segmentation in Section 2. Results, validation studies, and conclusions are given in Section 3 and Section 4.

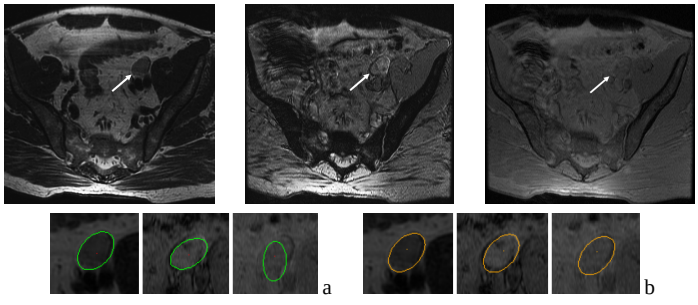

Fig. 2. The lymph node shows very different region and boundary characteristics in T2, T2* gradient echo 1 and 2 images (top from left to right). (a)Uncoupled segmentation (b)Coupled segmentation.

2. COUPLED ELLIPTICAL FLOWS

2.1. Region-Based Ellipse Evolutions

Given a finite number of images $I_i : \Omega_i \longrightarrow \mathbb{R}^{n\in\{2,3\}},\ i = 1,\ldots,m$, the goal is to find a contour $\mathbf{C} \in \Omega$ that propagates on an independent domain Ω whereas a contour $\boldsymbol{C^i}$ corresponding to the mapping $\boldsymbol{C^i} = g_i(\boldsymbol{C})$ propagates on the i^{th} image domain Ω_i with a region–based energy:

$$E(\boldsymbol{C}, g_1, ..., g_m) = \sum_{i=1}^{m} \int_{\boldsymbol{C_{in}^i}} f^i(g_i(x))|g_i'|dx \qquad (1)$$

where g_i' denotes the Jacobian of g_i, $f^i = f^i_{in} - f^i_{out}$, and f^i_{in} and f^i_{out} are the region descriptors inside and outside the transformed contour $g_i(\mathbf{C})$ respectively ($x \in \Omega_i$). A piecewise constant model for the target regions can be utilized by choosing $f^i = (I_i - \text{mean}_{\text{in}})^2 - (I_i - \text{mean}_{\text{out}})^2$ as in [16]. The evolution of the contour $\mathbf{C}$ is given by : $\frac{\partial \boldsymbol{C}}{\partial t} = \sum_{i=1}^{m} f^i(g_i(x))|g_i'|\boldsymbol{N}$, where $\boldsymbol{N}$ denotes the unit normal to $\boldsymbol{C}$ [10]. The ellipse flows will eliminate the need for a regularization on the unknown contour $\mathbf{C}$, which shrinks $\mathbf{C}$ with a speed depending on its curvature κ.

The parametrization of a 2D elliptical contour $\boldsymbol{\epsilon}(p)$ by $p \in [0, 2\pi)$, given its translation vector $\boldsymbol{t} = (d,\ e)^T$, rotation angle θ_e, and radii a and b, is given by:

$$\boldsymbol{\epsilon}(p) = a \begin{pmatrix} \cos\theta_e \\ -\sin\theta_e \end{pmatrix} \cos p + b \begin{pmatrix} \sin\theta_e \\ \cos\theta_e \end{pmatrix} \sin p + \begin{pmatrix} d \\ e \end{pmatrix}. \qquad (2)$$

Utilizing this parametrization, the variation of the energy in Eq. (1) w.r.t. ellipse parameters $\lambda^j \in \{a, b, d, e, \theta_e\}, j = 1,\ldots,5$ yields the gradient flows:

$$\frac{d\lambda^j}{dt} = \sum_{i=1}^{m} \oint_{\boldsymbol{\epsilon}} f^i(g_i(x))\langle \frac{\partial g_i(x)}{\partial \lambda^j}, g_i(x)\boldsymbol{N}\rangle |g_i'|dp \qquad (3)$$

for an evolution of the ellipse ($\oint_{\boldsymbol{\epsilon}}$ denotes an integration along the ellipse). The variation of the ellipse with respect to its parameters $\partial\boldsymbol{\epsilon}/\partial\lambda^j$ are computed by taking the partial derivatives of the ellipse equation in Eq.(2) with respect to each of the five parameters. In addition, for each of the rigid registrations g_i, we have $(g_i)_k = w_k$, $k = 1, ..., 4$ for two parameters of translation vector $\boldsymbol{T}$, one parameter of rotation matrix $\boldsymbol{R}$, and one parameter for uniform scale s. Similarly, we derive the variation of the rigid registration $\partial \boldsymbol{g}_i(x)/\partial w^k$ with respect to each w^k. In the end our goal is to obtain a set of equations to evolve the registration parameters, and to evolve the ellipse parameters, both based on region and edge-based energy terms as shown next.

2.2. Edge-based Ellipse Evolutions

The total edge-based energy of an ellipse can be given by:

$$E(\boldsymbol{\epsilon}, g_1, ..., g_m) = \sum_{i=1}^{m} \oint_{\boldsymbol{\epsilon}} \Phi^i(g_i(x))\|g_i'(\boldsymbol{\epsilon}_{\mathbf{p}})\|dp \qquad (4)$$

where Φ is a weighting function that is usually designed to slow down the propagation of the contour at high image gradients. Taking the derivative of the energy w.r.t. an independent time variable t yields the evolution:

$$\frac{\partial \lambda^j}{\partial t} = \sum_{i=1}^{m} \oint_{\boldsymbol{\epsilon}} \langle \nabla \Phi^i(g_i(x)) - \Phi^i(g_i(x)) \boldsymbol{T}^i_p, \frac{\partial g_i(x)}{\partial \lambda^j} \rangle \|g_i'(\boldsymbol{\epsilon}_p)\| dp \tag{5}$$

of the ellipse parameters λ^j, where $\boldsymbol{T}_p$ is the derivative of the tangent vector along the ellipse. Taking a closer look at this flow, one can note the similarity to the geodesic contour flow [17], where the second term in the inner product is the curvature term weighted by the conformal factor Φ, and the first term is the gradient of the conformal factor which pulls the contour back to the real boundary. In the above equation though, the integration around the ellipse provides a significant increase in robustness of the flow, allowing the contour to escape from local minima more easily, in contrast to a generic contour with geodesic energy.

Similarly, the evolution of the registration g_i can be obtained as follows:

$$\frac{\partial (g_i)_k}{\partial t} = \frac{\partial E}{\partial (g_i)_k} = \oint_{\boldsymbol{\epsilon}} \langle \nabla \Phi^i(g_i(x)), \frac{\partial g_i(x)}{\partial w_k} \rangle \|g_i'(\boldsymbol{\epsilon}^i_p)\| dp. \tag{6}$$

2.3. Combined Region and Edge-Based Ellipse Flows

We utilize a combination of the region and edge-based flows to obtain the update equations for both the registration and the segmentation of the ellipse as follows:

$$\frac{\partial (g_i)_k}{\partial t} = \oint_{\boldsymbol{\epsilon}} \langle [\nabla \Phi^i(g_i(x)) + f^i(g_i(x)) g_i \boldsymbol{N}], \frac{\partial g_i(x)}{\partial w_k} \rangle \|g_i'(\boldsymbol{\epsilon_p})\| dp, \tag{7}$$

$$\frac{\partial \lambda^j}{\partial t} = \sum_{i=1}^{m} \oint_{\boldsymbol{\epsilon}} \langle \frac{\partial g_i(x)}{\partial \lambda^j}, [\nabla \Phi^i(g_i(x)) + f^i(g_i(x)) g_i \boldsymbol{N}] \rangle \|g_i'(\boldsymbol{\epsilon_p})\| dp \tag{8}$$

for the k^{th} parameter of the registration, $k = 1, \ldots, 4$, and the j^{th} parameter of the segmentation $j = 1, \ldots, 5$, and for the i^{th} transformation corresponding to image I_i.

3. RESULTS

We demonstrate the algorithm's application to a dataset from MR scans of prostate cancer screening studies. The image modalities used are post-contrast T2, T2* echoes 1 and 2. An initialization of a region of interest (ROI) box, i.e. a rectangle, in a slice of one of the volumes triggers a deformable contour initialization, particularly an ellipse contour. The algorithm propagates in 2D space on all modalities, then extends to other slices in 3D. We show here 2D slices in many of the examples for simplicity of discussion.

In Fig. 3, a benign lymph node is merged with the vessels next to it, therefore this example presents a challenge for a contour that evolves without any shape constraints. This is shown at the top where a level-set based active contour that uses region- and edge-based speed terms is utilized. The ellipse-based evolutions on the other hand successfully segment the lymph node region of interest. Similarly, for the malignant node on the right, an active contour method is distracted by the dark spot in the lymph node and has trouble in

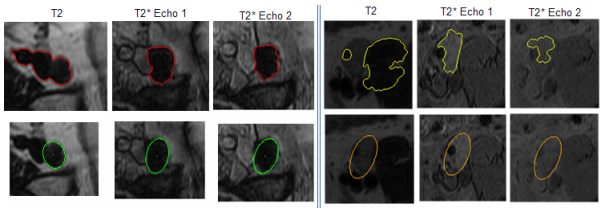

Fig. 3. The active contour leaks to neighboring vessel regions, and fails to delineate the benign node (row 1 left) and the malignant node (row 1 right) as opposed to the ellipse (row 2).

	Benign LN Example			Malignant LN Example		
Setting	T2	T2*1	T2*2	T2	T2*1	T2*2
Level set contour based	1562	291	199	1716	1609	807
Ellipse based	246	267	200	425	217	493

Table 1. Number of non-overlapping pixels with respect to manual segmentation for active contour vs. ellipse based segmentation and registration.

estimating the real boundaries in all sequences in contrast to the ellipse propagation. In Table 1, we display the total number of pixels that are non-overlapping with the manual segmentation map for both the active contour segmentation and the ellipse segmentation map summed over the 2D slices of the lymph nodes. It can be observed from the numbers in the table that the coupled ellipse flows produce much better results than that of the active contour due to constrained motion of the former.

We have 30 lymph node samples taken from 7 patients, of which 17 are benign and 13 are malignant. We show the semi-automatic segmentation results from this dataset in Fig. 4. Out of the 30 lymph node boundary delineations, two malignant node results were not exact and stayed inside the node without expanding. With the contrast-agent penetration, the metastatic tumors are expected to stay light in intensity and exhibit a homogeneous region character, however this may not be true in all cases. Malignancy may exhibit a partial infiltration, hence a complex texture in T2* echo images, therefore the full delineation of node boundaries may be harder. For the classification of tumors based on nodal intensity changes inside the node though, even a partial delineation may be useful. To assess the region delineation performance, in Table 2, we display the error of omission (Type I error) and the error of commission (Type II error) between the manual segmentation (by an ellipse) and the automatic ellipse segmentation given an ROI for each of the 30 lymph nodes in our initial data set. It can be observed that the noisier modality, particularly T2* echo 2, results in a higher percentage of error whereas the T2 and T2* echo 1 exhibit around $10 - 15\%$ error of omission. These results show that the coupled ellipse flows provide a reasonable nodal region delineation for later feature extraction and diagnosis stages.

From the segmented lymph nodes, we automatically extract lymph node features proposed in the work of Harisinghani and Weissleder [1] such as the lymph node variance, lymph node size, roundedness, and a specific T2 star value based on the mean nodal intensity inside the lymph node. We output these features for the lymph node classification stage

	T2		T2*1		T2*2	
Percent Error	avg	std	avg	std	avg	std
Err. Omission	11.00	11.97	13.05	15.39	19.96	19.95
Err. Commission	23.03	17.29	21.80	17.13	27.70	25.07

Table 2. Summary of validation statistics (average and standard deviation values): Percent error of omission (Type I error) and percent error of commission (Type II error) between the algorithm and manual segmentations.

that uses a Bayesian network model [18]. In addition, for surgical planning, the visualization of the lymph nodes with respect to the vascular anatomy of the patient is performed through the MR-T1 scan as shown in Fig. 5.

For more in depth validation, a bigger database of approximately 300 patients will be acquired, and classification of lymph nodes with features extracted from the lymph nodes delineated by our technique will be carried out.

4. CONCLUSIONS

We presented an application-specific lymph node segmentation and feature extraction system, which couples the information from MR T2-, and multiple T2*-weighted images for a joint segmentation and registration. We hence simultaneously capture the boundaries of the lymph node in all the image volumes. For surgical planning, we obtain a segmentation in 3D and output the final lymph node surface for visualization along with the vascular anatomy using the MR T1 volume. We also automatically extract the lymph node features for lymph node classification. Current results have shown that the coupled elliptical registration and segmentation is useful and will assist in delineation of lymph nodes from multiple MRI sequences, and in assessment of lymphatic spread for accurate staging of cancer and surgical planning.

5. REFERENCES

[1] M. Harisinghani and R. Weissleder, "Sensitive, noninvasive detection of lymph node metastases," *PLOS Medicine*, vol. 1, no. 3, 2004.

[2] M. Harisinghani, J. Barentsz, P.F. Hahn, W. M. Deserno, S. Tabatabaei, C. Hulsbergen van de Kaa, J. de la Rosette, and R. Weissleder, "Noninvasive detection of clinically occult lymph-node metastases in prostate cancer," *The New England Journal of Medicine*, vol. 348, no. 25, pp. 2491–2499, 2003.

[3] T. McInerney and D. Terzopoulos, "Deformable models in medical image analysis: A survey," *Medical Image Analysis*, vol. 1, no. 2, pp. 91–108, 1996.

[4] S. Birchfield, "Elliptical head tracking using intensity gradients and color histograms," in *IEEE Int. Conf. Computer Vision and Pattern Recognition*, 1998.

[5] N.Grammalidis and M.G.Strintzis, "Head detection and tracking by 2-d and 3-d ellipsoid fitting," in *IEEE Computer Graphics International Conference*, 2000.

[6] J.A.K. Blokland, A.M. Vossepoel, A.R. Bakker, and E.K.J. Pauwels, "Delineating elliptical objects with an application to cardiac scintigrams," *IEEE Trans. Medical Imaging*, vol. 6, no. 1, 1987.

[7] L. Staib and J. Duncan, "Model-based deformable surface finding for medical images," *IEEE Trans. on Medical Imaging*, vol. 15, no. 5, pp. 720–731, 1996.

[8] C. Brechbuhler, G. Gerig, and O. Kubler, "Parametrization of closed surfaces for 3-d shape description," *Computer Vision and Image Understanding*, vol. 61, no. 2, pp. 154–170, 1995.

[9] J.B.A. Maintz and M.A. Viergever, "A survey for medical image registration," *Medical Image Analysis*, vol. 2, no. 1, pp. 1–36, 1998.

[10] A. Yezzi, L. Zollei, and T. Kapur, "A variational framework for joint segmentation and registration," in *CVPR-MMBIA*, 2001, pp. 44–49.

[11] N. Paragios, N. Rousson, and M. Ramesh, "Knowledge-based registration and segmentation of the left ventricle," in *IEEE Workshop on App. Comp. Vision*, 2002.

[12] B. Vemuri and Y. Chen, "Joint image registration and segmentation. In: Geometric level set methods in imaging, vision and graphics," 2003, pp. 251–269, Springer.

[13] P. Wyatt and J. Noble, *MAP MRF Joint Segmentation & Registration*, MICCAI, 2002.

[14] I. Dydenko, D. Friboulet, and I.E. Magnin, "A variational framework for affine registration and segmentation with shape prior: application in echocardiographic imaging," in *VLSM-ICCV*, 2003, pp. 201–208.

[15] A. Wong, H. Liu, A. Sinusas, and P. Shi, "Spatiotemporal active region model for simultaneous segmentation and motion estimation of the whole heart," in *VLSM Workshop-ICCV*, 2003.

[16] T.F. Chan and L.A. Vese, "An active contour model without edges," in *Scale-Space*, 1999.

[17] S. Kichenassamy, A. Kumar, P. Olver, A. Tannenbaum, and A. Yezzi, "Gradient flows and geometric active contours," in *Proc. ICCV*, 1995, pp. 810–815.

[18] T. Fuchs, B. Wachmann, J. Cheng, C. Neubauer, J. Tyan, R. Krieg, C.P. Schultz, R. Seethamraju, M.G. Harisinghani, and R. Weissleder, "A bayesian network model for lymph node classification," 2005, Siemens Corporate Research Tech. Report.

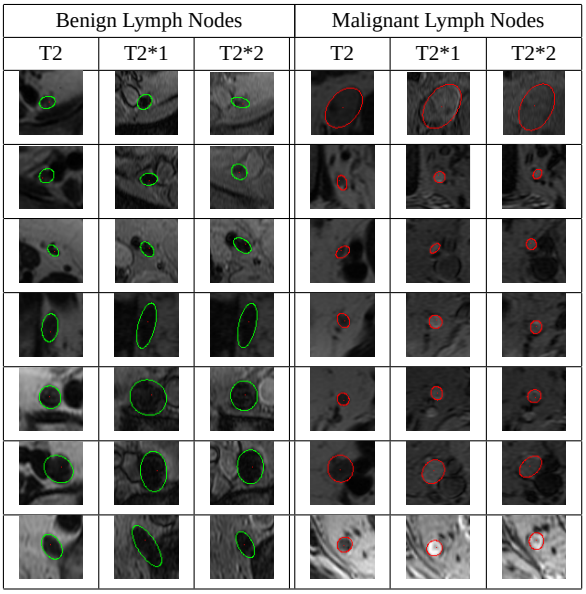

Fig. 4. Lymph node examples from the database.

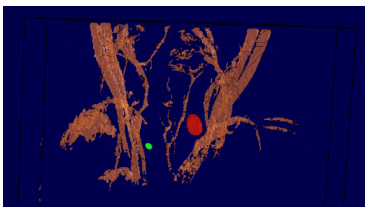

Fig. 5. 3D visualization of a benign (small green) and a malignant (big red) lymph node along with vascular anatomy aids in surgical planning.